The latest version is at http://www.jbc.org/cgi/doi/10.1074/jbc.M113.467753

Determinants of 14-3-3σ dimerization and function in drug and radiation resistance*

Zhaomin Li[1], Hui Peng[1,‡], Li Qin[1], Jing Qi[1], Xiaobing Zuo[2], Jing-Yuan Liu[1,3], Jian-Ting Zhang[1,4]

From the [1]Department of Pharmacology and Toxicology, Indiana University School of Medicine, Indianapolis, IN 46202; [2]X-Ray Science Division, Argonne National Laboratory, Argonne, IL 60439; [3]Department of Computer and Information Science, Indiana University-Purdue University, Indianapolis, IN 46202. [4]IU Simon Cancer Center, Indiana University School of Medicine, Indianapolis, IN 46202;

Running Title: *14-3-3σ dimerization and function*

Address all correspondence to J.T. Zhang, IUSCC, R3-C570, 980 W. Walnut Street, Indianapolis, IN 46202. Tel. 317-278-4503; Fax 317-274-8046; E-mail: jianzhan@iupui.edu or J.Y. Liu, 723 W. Michigan St., SL280C, Indianapolis, IN 46202. Tel: (317) 274-7645; Fax: (317) 274-1560; E-mail: jliu2@iupui.edu.

Keywords: 14-3-3σ, drug and radiation resistance, dimerization, MD simulation

Background: 14-3-3σ is a homo-dimeric protein important for drug and radiation resistance.
Results: Mutation of single hydrophobic core residue results in non-functional monomeric proteins.
Conclusion: Hydrophobic core residues are important for 14-3-3σ dimerization and homo-dimerization is required for its function.
Significance: Identifying important hydrophobic core residues for homo-dimerization may help drug the "undruggable" protein dimers such as 14-3-3σ.

SUMMARY

Many proteins exist and function as homo-dimers. Understanding the detailed mechanism driving the homo-dimerization is important and will impact future studies targeting the "undruggable" oncogenic protein dimers. In this study, we used 14-3-3σ as a model homo-dimeric protein and performed a systematic investigation of the potential roles of amino acid residues in the interface for homo-dimerization. Unlike other members of the conserved 14-3-3 protein family, 14-3-3σ prefers to form homo-dimer with two subareas in the dimeric interface that has 180° symmetry. We found that both subareas of the dimeric interface are required to maintain full dimerization activity. While the interfacial hydrophobic core residues Leu[12] and Tyr[84] play important roles in 14-3-3σ dimerization, the non-core residue Phe[25] appears to be more important in controlling 14-3-3σ dimerization activity. Interestingly, a similar non-core residue Val[81] is less important than Phe[25] in contribution to 14-3-3σ dimerization. Furthermore, dissociating dimeric 14-3-3σ into monomers by mutating the dimerization residues Leu[12], Phe[25], or Tyr[84] individually diminished the function of 14-3-3σ in resisting drug-induced apoptosis and in arresting cells at G_2/M phase in response to DNA-damaging treatment. Thus, dimerization appears to be required for the function of 14-3-3σ.

14-3-3σ is a member of the highly conserved mammalian 14-3-3 protein family that function as chaperons (1-3) and bind to a variety of proteins important for various cellular processes (4) including cytokinesis (5), cell cycle regulation (6-9), and apoptosis (8,10-12). Because of its roles in multiple cellular processes, 14-3-3σ has been

This is the author's manuscript of the article published in final edited form as:
Li, Z., Peng, H., Qin, L., Qi, J., Zuo, X., Liu, J. Y., & Zhang, J. T. (2013). Determinants of 14-3-3σ Protein Dimerization and Function in Drug and Radiation Resistance. Journal of Biological Chemistry, 288(44), 31447-31457.
http://dx.doi.org/10.1074/jbc.M113.467753

considered as a double-edged sword of cancers (1). Silencing the expression of 14-3-3σ may contribute to tumorigenesis (13,14) while its up-regulation in cancers causes resistance to chemotherapy (8,15,16).

The atomic structure of 14-3-3σ has been determined (4,17) to have an overall dimeric structure that resembles a flattened horseshoe (1). Each subunit of the dimer consists of 9 α-helices. Unlike most other 14-3-3 proteins that can form both homo- and hetero-dimers among the 14-3-3 family proteins, 14-3-3σ prefers to form only homo-dimers (17). It has also been found that mutation of Ser^{5}, Glu^{20} and Glu^{80} residues promoted hetero-dimerization of 14-3-3σ with other 14-3-3 isoforms while mutations of the Phe^{25} and Gln^{55} residues promoted little hetero-dimerization although they decreased the ability of 14-3-3σ to form homo-dimers (18). Interestingly, the combined mutations of all five residues resulted in a mutant that could no longer form homo-dimer but could form hetero-dimers with all other six 14-3-3 isoforms.

In a recent study analyzing mechanisms of 14-3-3σ dimerization using molecular dynamic (MD) simulations and site-directed mutagenesis (19), we found that Phe^{25} is critical in packing and stabilizing hydrophobic core residues that are important for dimerization by organizing co-operativity of core and other residues for favorable hydrophobic and electrostatic interactions. This organizing activity of Phe^{25} for 14-3-3σ homo-dimerization is bestowed from its unique physical location, rigidity, size, and hydrophobicity.

In this study, we performed a systematic study of the amino acid residues in the hydrophobic core of the 14-3-3σ dimeric interface along with residues not located in the hydrophobic core for their potential role in 14-3-3σ dimerization and investigated the potential effect of the mutations of these residues on 14-3-3σ function. We have identified amino acid residues that are important to maintain the dimerization activity of 14-3-3σ and shown that dimerization is required for the function of 14-3-3σ in contributing drug and radiation resistance.

Experimental Procedures

Cell culture and transfection. HEK293 cells were cultured in DMEM supplemented with 10% fetal bovine serum [Invitrogen] and 1% penicillin/ streptomycin [BioWhittaker]. Mia PaCa-2 cells were cultured in DMEM supplemented with 10% fetal bovine serum, 2.5% equine serum [Hyclone] and 1% penicillin/streptomycin. Transient and stable of 14-3-3σ transfection were performed with Lipofectamine [Invitrogen] as we previously described (20). Stable transfectants were generated by selection using 1mg/ml G418 for 2 weeks and then single clones were selected and maintained in the presence of 200ug/ml G418. The protein levels of 14-3-3σ in the stable clones were continuously monitored using Western blot.

Construct engineering. Wild type and mutant 14-3-3σ constructs with different tags (Flag, HA, Myc, and HAM_2) were engineered using PCR and QuickChange® Site-Directed Mutagenesis Kits as we previously described (8,15,19-21). The primer pairs used for each construct are shown in Table 1.

In-vitro transcription and translation. In-vitro transcription and translation were performed as previously described (22,23). Briefly, 14-3-3σ constructs were linearizated using XhoI, followed by *in vitro* transcription using T7 RNA polymerase. The in-vitro transcripts were then purified and used to program cell-free translation in rabbit reticulocyte lysate. The reactions were stopped by incubation at 65°C for 5min and subjected to co-immunoprecipitation and Western blot analysis.

Immunoprecipitation and Western blot analysis. Immunoprecipitation and Western blot analysis were performed as previously described (19,24,25). Briefly, cell lysates or *in vitro* translation products were precleared with protein A beads plus normal mouse IgG followed by incubation with primary HA (Convance), Myc (Cell Signaling), or Flag (Sigma) antibodies and protein A beads. The precipitated materials were washed extensively with with TNN buffer (50mM Tris·HCl, PH7.4, 150mM NaCl, 5% NP-40, 20mM EDTA, 50mM NaF, 1mM Na3VO3, 1mM PMSF, 1mM DTT). The final precipitated materials were pelleted by centrifugation and solubilized for separation on SDS-PAGE followed by Western blot analysis probed using HA, Myc, Flag, or actin (Santa Cruz) antibodies. The images were captured with FlourchemHD2 (Alpha Innotech corporation) after incubated with ECL (GE).

Survival assay. Survival assay was performed as previously described using SRB (sulforhodamine B) or colony formation assays (20,26). Briefly, for SRB assay, 5000 cells/well were seeded in 96-well plates and cultured overnight. The cells were then treated with various concentrations of mitoxantrone for three days followed by incubation with 0.4% (W/W) sulforhodamine B in 1% Acetic Acid (V/V) for 30 minutes at room temperature. Unbound sulforhodamine B was then removed by washing with 1% acetic acid for three times and cells were air dried. Finally, the bound sulforhodamine B was solubilized with in 10 mM Tris base and OD_{570nm} was measured. For colony formation assay, cells were seeded 100 cells/well in 6 well plates and cultured overnight. The cells were then treated with 2 Gy γ-irradiation followed by continuous culture for two weeks with media changed every 2-3 days. Cell colonies were stained with crystal violet and counted manually. Survival data was analyzed with GraphPad Prism 4.

Cell cycle analyses. Cell cycle analysis was performed with propidium iodide (PI) staining and FACS as previously described (27). Briefly, 3×10^5cells were seeded in a 6-cm dish followed by treatment with 10 nM mitoxantrone or DMSO for three days. Cells were then collected and fixed in cold 75% ethanol and stained with 100ug/mL propidium iodide, followed by analysis with FACS (fluorescence-activated cell sorting). The data were analysed using Cell Quest and Modifit programs.

Molecular Modeling and MD simulation. The structure with Pdb code 1YWT from protein databank was used as the template structure for 14-3-3σ and missing loops were modeled by MOE with the homology modeling module. Mutations of specific residues were introduced by the UCSF Chimera swapaa function. MD simulations of mutant 14-3-3σ dimers were carried out using the AMBER9 package. FF03 parameters and hydrogen atoms were assigned to the protein by tleap module of AMBER9. All dimers were solvated in a 84 x 103 x 67 Å rectangular box. Appropriate number of counter ions was added to neutralize each system. Particle Mesh Ewald (PME) was employed to calculate the long-range electrostatic interactions and the nonbonded cutoff was set to 8.0 Å.

Each system was equilibrated by a four-step protocol prior to production MD simulation as previously described (19). The same conditions of the final equilibration step were used for 20-ns production MD simulations.

To determine how each mutation affects 14-3-3σ dimerization, binding free energies between the two associating subunits were calculated using the GBSA method (28). The binding free energy is computed by taking the difference between the mm-GBSA free energy of the complex with that of the ligand and receptor: $\Delta G_{bind}=G_{complex}-G_{receptor}-G_{ligand}$, where

$G=G^{solute}+G^{solvent}$. The G^{solute} term for each system can be obtained by $G^{solute}=E-TS$. E represents an average of energies obtained from MD simulation and is the sum of the following 3 terms: "non-bonded electrostatic energy + 1,4-electrostatic energy" (E^{ele}); "non-bonded van der Waals energy + 1,4-van der Waals energy" (E^{vdw}) and "bond, angle, dihedral energies" (E^{int}). S is the entropy contribution that is omitted from our calculation because the purpose of this study is to compare the effect of each mutation on dimerization rather than to calculate absolute binding free energy. The $G^{solvent}$ term can be obtained by $G^{solvent}=G^{es}+G^{nes}$. G^{es} is the electrostatic contribution that is obtained by the GB method, and G^{nes} is the non-electrostatic contribution and is proportional to the solvent-accessible surface area of the molecule. As the entropy term is not included in this study, the calculated total binding free energy (ΔGbind) only consists of the E and $G^{solvent}$ terms. A total of 100 snapshots were collected from the production trajectory for MM-GBSA free energy calculations. Grid size was set as 0.5 Å, and the dielectric constants for the solute and solvent were set as 1 and 80, respectively. RMSF of interfacial core residues were calculated by the atomicfluct command of ptraj.

Small-angle x-ray scattering (SAXS) analysis. SAXS was performed using beamline 12ID-B of Advanced Photon Sources (APS) at Argonne National Laboratory. The wavelength, λ, of x-ray radiation was set as 0.866 Å. Scattered x-ray intensities were measured using two detectors, Pilatus 2M and 300K (DECTRIS Ltd). The sample-to-detector distance was set such that the detecting range of momentum transfer q (=4π sinθ/λ, where 2θ is the scattering angle) of SAXS experiments was 0.01-2.6 $Å^{-1}$. To reduce the radiation damage, a flow cell made of a cylindrical quartz capillary with a diameter of 1.5 mm and a wall of 10 μm was used and the exposure time was set to 1 second. In order to obtain good signal-to-noise ratios, twenty images were taken for each sample and buffer control. The 2-D scattering images were converted to 1-D SAXS curves through azimuthally averaging after solid angle correction and then normalization with the intensity of the transmitted x-ray beam. The software package used for the conversion was developed at beamline 12ID-B. Undesired interactions among biomacromolecules have been corrected, if any, before data analysis. The radius of gyration (Rg) was calculated using the Guinier equation $I(q) = Io\exp(-R_g^2q^2/3)$, where Io is the forward scattering (29). The pair distance distribution function (PDDF) that is roughly a weighted histogram of atomic-pair distance in the molecule, were calculated using GNOM (30).

Results

Analysis of the dimeric interface of 14-3-3σ. To investigate the determinant residues of 14-3-3σ dimerization, we first examined the dimeric interface of 14-3-3σ (PDB code: 1YZ5 and 1YWT). The overall structure of 14-3-3σ dimer is composed of nine helices, A through I, from each monomer (4,5). Helices A and B of one subunit interact with helices C and D of the opposing subunit, respectively, and *vice versa*. The 980 $Å^2$ total buried interface can be divided into two structurally similar subareas, which are related by the pseudo-2-fold symmetry of the protein (19). In each subarea, residues Lys^9, Leu^{12}, Ala^{13} and Ala^{16} of one subunit and Ala^{58}, Leu^{62}, Tyr^{84} and Val^{88} of the opposing subunit form an interfacial core as defined previously (19) and all have >80% buried surface area in the dimeric interface (solvent accessible area in monomeric protein that becomes buried upon dimerization) (Table 2). The top two most buried core residues, Tyr^{84} and Leu^{12}, have 99 and 96% of their solvent accessible area buried in the dimeric interface, respectively,

and provide the highest level of buried surface areas (120 and 88 Å^2, respectively).

Contribution of Leu^{12}, Phe^{25}, Val^{81} and Tyr^{84} to 14-3-3σ dimerization. To investigate the potentially important residues in 14-3-3σ dimerization, we chose to further investigate the top two core residues, Tyr^{84} and Leu^{12}. We also selected two other hydrophobic residues, Phe^{25} and Val^{81}, which have 40-50% of its solvent accessible area buried in the dimeric interface (Table 2) but are not located in the interfacial core. Gln^{8}, which does not appear to contribute to dimerization from our analysis was chosen as a negative control residue.

Next, all five residues were mutated to Gly since MD simulations have shown previously that the L^{12}G, F^{25}G, and Y^{84}G mutations do not interrupt the stability of the helices they reside on despite that Gly is a potential helix breaker (19). A 3-ns MD simulation of the V^{81}G and Q^{8}G mutants also shows that these mutations do not disrupt the stability of their respective helices (data not shown). Therefore, the secondary structure of α-helices in these mutants may be maintained as in the wild type protein (see also below).

Because the dimeric 14-3-3σ structure has an 180^{o}-symmetry and each interfacial residue occurs twice, each residue contributes to two interactions with one from each subunit in two interfacial subareas (Fig. 1A). To determine the potential contribution of Leu^{12}, Phe^{25}, Val^{81} and Tyr^{84} to 14-3-3σ dimerization, we performed an experiment to determine if the mutant 14-3-3σ can dimerize with the wild type one using co-immunoprecipitation. In this case, only one of the two interfacial subareas carries a mutation in the mutant subunit. We first engineered wild type 14-3-3σ tagged with an HA epitope (σ-HA, Fig. 1A) and mutant 14-3-3σ tagged with an HA and two Myc epitopes (σ-HAM$_2$, Fig. 1A), for convenience of detecting both wild type and mutant proteins using a common HA antibody and to differentiate them by ~3-kDa difference in size on Western blot. Next, we transiently transfected the HAM$_2$-tagged mutant constructs into HEK-293 cells with stable expression of HA-tagged wild type 14-3-3σ. As shown in Fig. 1B (input), all HAM$_2$-tagged mutant constructs were well expressed along with the HA-tagged wild type 14-3-3σ. Co-immunoprecipitation was then performed using Myc antibody followed by Western blot analysis of the precipitate using HA antibody. Fig. 1B shows that HAM$_2$-tagged Q^{8}G and wild type 14-3-3σ co-precipitate HA-tagged wild type 14-3-3σ whereas the HAM$_2$-tagged L^{12}G, F^{25}G, and Y^{84}G mutants do not.

Surprisingly, the HAM$_2$-tagged V^{81}G mutant also co-precipitated the HA-tagged wild type 14-3-3σ. Because Val^{81} and Phe^{25} have similar buried surface area in dimeric interface (25 Å^2 and 24 Å^2, respectively) and these buried areas also occupy similar percentages (53% and 42%, respectively) of their total solvent accessible areas in the monomeric protein (Table 2), their contribution to dimerization was thought to be similar. However, this is clearly not the case as V^{81}G but not F^{25}G co-precipitated the wild type 14-3-3σ.

To eliminate the possibility that above observations of 14-3-3σ dimerization is due to stable cell lines used, these constructs were used to program cell-free transcription and translation followed by co-immunoprecipitation using Myc antibody and Western blot analysis using HA antibody. As shown in Fig. 1C, similar findings of co-precipitation were observed with the HAM$_2$-tagged wild type, Q^{8}G and V^{81}G mutants while no co-precipitation was observed with HAM$_2$-tagged L^{12}G, F^{25}G, and Y^{84}G mutants. Thus, the differential dimerization activity of mutant 14-3-3σ is unlikely due to cell line or cell-free systems used.

To further confirm the above observations, we next used a different

method of detection and performed a non-denaturing PAGE separation of cell-free translation products of HA and HAM_2-tagged wild type and $F^{25}G$ mutant 14-3-3σ followed by Western blot analysis probed with HA and Myc antibodies. To rule out the possible effect of mutation to Gly residue, we also created another mutant, $F^{25}E$, for analysis. As shown in Fig. 2, HAM_2- and HA-tagged wild type 14-3-3σ each alone formed a dimer with highest (HAM_2/HAM_2) and lowest (HA/HA) molecular weight, respectively (lanes 1 and 4, top panel). Co-translation of both HAM_2- and HA-tagged wild type 14-3-3σ formed hetero-dimers (HAM_2/HA) between the two differentially tagged 14-3-3σ molecules with a mobility between HAM_2/HAM_2 and HA/HA homo-dimers (lane 5). However, $F^{25}G$ and $F^{25}E$ mutants alone could not form any detectable dimer by themselves (lanes 2-3). Furthermore, co-translation of wild type and mutant 14-3-3σ generated only dimers of the HA-tagged wild type protein while the HAM_2-tagged mutant 14-3-3σ stayed as monomers (lanes 6-7). Thus, we conclude that wild type 14-3-3σ likely prefers to bind to wild type 14-3-3σ and the Phe^{25} mutant 14-3-3σ does not have affinity to the wild type protein or itself and that the mutation effect on dimerization is unlikely due to Gly residue used as a substitute residue.

$V^{81}G$ mutation does not cause changes to the hydrophobic core residues in the dimeric interface of 14-3-3σ. Previously, we have shown that the important role of Phe^{25} in 14-3-3σ dimerization is due to its physical location, rigidity, size, and hydrophobicity although it is not located in the hydrophobic core. Mutation of Phe^{25} in both subunits results in loosely-packed cores, which lead to lost affinity between the two opposing subunits.

Because Val^{81} and Phe^{25} both have similar total and percentage of surface areas that become buried upon dimerization as discussed above (see also Table 2), it is of interest to investigate the structural basis for the difference between Phe^{25} and Val^{81} in contributing to dimerization. For this purpose, we performed 20-ns MD simulations of both $WT/V^{81}G$ and $WT/F^{25}G$ dimers as well as WT/WT dimer followed by calculation of the total binding free energies. Because the purpose of the study is for comparison between wild type and mutant proteins, we omitted the entropy term. The calculated total binding free energy represents only the enthalpy term. While $WT/V^{81}G$ has a total calculated binding free energy of -35.49 kcal/mol, which is comparable to the total binding free energy of WT/WT at -39.77 kcal/mol, the calculated binding free energy of $WT/F^{25}G$ is much higher at -27.81 kcal/mol (19).

To investigate the effect of mutations on the stability of the core residues, root mean square fluctuation (RMSF) of each core residue including atoms on both main and side chains were calculated from the simulations. As shown in Fig. 3, although $F^{25}G$ mutation was introduced into only subunit II, which directly affected core II consisting of A^{58}, L^{62}, Y^{84} and V^{88} of subunit I and K^{9}, L^{12}, A^{13} and A^{16} of subunit II, the stability of residues in core I was also affected. As a result, the average RMSF of core residues in $WT/F^{25}G$ is 0.66. In contrast, the core residues of $WT/V^{81}G$ and WT/WT dimers are stable and both have the same lower average RMSF of 0.56.

Dimerization of 14-3-3σ with mutations in both dimeric interfaces. In above studies using co-immunoprecipitation of two differentially tagged proteins, we found that $L^{12}G$, $F^{25}G$, and $Y^{84}G$ mutants could not dimerize with the wild type 14-3-3σ. However, in our computational analyses of the mutant 14-3-3σ, we found that both $L^{12}G$ and $Y^{84}G$ mutants appear to have some affinity to itself (19). Thus, we next tested if these mutant 14-3-3σ can form homo-dimers or dimerize with other mutants to form

hetero-dimers. These possible combinations of dimers carry the same or different mutations in one or both interfacial cores (Fig. 4A). For this purpose, Myc-tagged $L^{12}G$, $F^{25}G$, and $Y^{84}G$ mutants were transiently transfected into the corresponding cells with stable expression of the same mutant tagged with Flag epitope followed by co-immunoprecipitation with Flag antibody and Western blot analysis with Myc and Flag antibody. As shown in Fig. 4B, the non-core mutant ($F^{25}G$) did not form any mutant homo-dimer, consistent with the finding using non-denaturing PAGE analysis shown in Fig. 3. However, the mutants of the hydrophobic core residues ($L^{12}G$ and $Y^{84}G$) formed homo-dimers with itself although formation of the mutant homo-dimers appeared to be less than the wild type homo-dimer (Fig. 4B).

We next determined dimerization between different mutants using the same approach as described above. As shown in Fig. 4C, the $L^{12}G/Y^{84}G$ dimer was detected albeit at lower level compared with wild type proteins. However, no $F^{25}G/L^{12}G$ or $F^{25}G/Y^{84}G$ hetero-dimers were detected. Together with the data shown in Fig. 4B, these observations suggest that $F^{25}G$ mutation completely eliminated its dimerization activity whereas $L^{12}G$ and $Y^{84}G$ mutants retained some of their activities to dimerize with itself or each other but not with wild type or $F^{25}G$ mutant 14-3-3σ. The lack of interaction between wild type and $L^{12}G$ or $Y^{84}G$ mutants may be due to the reduced dimerization activity of the mutants which cause unfavorable kinetics in dimerization with and competing for the wild type molecules which have higher affinity for itself (see Discussion below).

Monomeric 14-3-3σ may not be functional. Previously, we found that over-expression of 14-3-3σ caused cellular resistance to anticancer drugs such as mitoxantrone and to γ-irradiation (8,15,20). The above studies showed that while wild type 14-3-3σ could form strong homo-dimers, the hydrophobic core mutants $L^{12}G$ and $Y^{84}G$ have weaker interactions and form much less homo-dimers compared with the wild type protein. The non-core $F^{25}G$ mutant, on the other hand, could not form any detectable homo-dimers. We next wanted to determine if the monomeric 14-3-3σ is functional. For this purpose, we first established stable PaCa-2 cell lines transfected with wild type or mutant 14-3-3σ with similar expression levels (Fig. 5A). These cell lines were then subjected to SRB assay to determine their relative resistance to mitoxantrone. As shown in Fig. 5B-C, expression of the wild type 14-3-3σ caused a 3-fold increase in resistance compared with the vector-transfected control cell that does not express any detectable 14-3-3σ, consistent with our previous findings (8,15,20). However, ectopic over-expression of $F^{25}G$ and $Y^{84}G$ mutants had no significant effect on cellular resistance to mitoxantrone. Interestingly, the stable cell line with $L^{12}G$ mutant had a low but significant resistance to mitoxantrone compared to the vector-transfected control cell. This observation is consistent with the fact that $L^{12}G$ has the most remaining dimerization activity among all three mutants. Together, these findings indicate that the monomeric mutant 14-3-3σ may not be functional in causing cellular resistance to anticancer drugs.

To further determine if monomeric 14-3-3σ is functional, we chose to analyze $F^{25}G$ as a representative in more detail in the following experiments. In a previous report, we showed that over-expression of 14-3-3σ contributes to resistance to γ-irradiation (20). To determine if 14-3-3σ-mediated radiation resistance also requires dimeric 14-3-3σ, we performed colonogenic assay following γ-irradiation using PaCa-2 cells with stable expression of wild type and $F^{25}G$ mutant 14-3-3σ. As shown in Fig. 5D, PaCa-2 cells with wild type 14-3-3σ were significantly more

resistant to γ-irradiation than the vector-transfected control cells. However, PaCa-2 cells expressing the mutant $F^{25}G$ had similar sensitivity to γ-irradiation as the vector-transfected control cells. Thus, dimerization is likely also required for the function of 14-3-3σ in resistance to γ-irradiation.

*Reduced function of monomeric 14-3-3σ in resisting drug-induced apoptosis and G_2/M arrest***.** Previously, it has been shown that the molecular basis of 14-3-3σ function in drug and radiation resistance is due to its role in regulating DNA-damage-induced apoptosis and cell cycle arrest (1). To determine if the monomeric mutant 14-3-3σ retains any of its function in cellular response to drug-induced apoptosis and G_2/M arrest, we treated PaCa-2 cell lines with stable expression of wild type and mutant 14-3-3σ as well as vector-transfected control cells with mitoxantrone and then determined cleavage of PARP, a target substrate of activated caspases. Fig. 6 shows a time course of production of the cleaved 85-kDa PARP fragment induced by mitoxantrone. It appears that the wild type as well as all mutant 14-3-3σ molecules could slow down the production of the 85-kDa PARP fragment compared with the vector-transfected control cells. At 6 hrs of mitoxantrone treatment, all PARPs have been cleaved in the vector-transfected control cells. At 9-hrs of treatment, the stable cells expressing $F^{25}G$ and $Y^{84}G$ mutants had >80% of PARPs cleaved. However, stable cells with wild type and $L^{12}G$ mutant had only ~50% PARPs cleaved following 9-hrs of mitoxantrone treatment. These observations suggest that the monomeric mutant 14-3-3σ has reduced activity to resist drug-induced apoptosis. The $L^{12}G$ mutant retains more activity in resisting drug-induced apoptosis than the other mutants, consistent with the observation that it maintains more dimerization activity than the other mutant molecules.

Next, we tested activity of the monomeric mutant 14-3-3σ in regulating G_2/M arrest in response to DNA damages. Following mitoxantrone treatment, PaCa-2 cell lines with stable expression of wild type and mutant 14-3-3σ as well as vector-transfected control cells were tested for their cell cycle distribution. As shown in Fig. 7A-B, all cells had similar cell cycle distribution under the control growth condition. However, following mitoxantrone treatment cells expressing wild type 14-3-3σ have ~51% cells arrested in G_2/M phase compared with ~24% of vector-transfected control cells. Cells expressing the mutant 14-3-3σ had ~36-42% cells in G_2/M phase with the $L^{12}G$ mutant having the highest G_2/M population among all mutant molecules. Thus, the monomeric mutant 14-3-3σ is less efficient than the wild type dimeric 14-3-3σ in arresting cells in G_2/M phase in response to DNA-damaging treatment.

Previously, it has been shown that 14-3-3σ arrests cells in G_2/M phase possibly by retaining cdc2 in cytoplasm (8). To determine if the mutant 14-3-3σ possibly lost this activity, we performed an indirect immunofluorescence staining of PaCa-2 cells with stable expression of wild type and $F^{25}G$ mutant 14-3-3σ. Fig. 7C shows that cdc2 is located in cytoplasm in both cells under control conditions. However, cdc2 moved into nucleus in cells with $F^{25}G$ mutant 14-3-3σ but remained in cytoplasm in the cells with wild type 14-3-3σ. This observation suggests that the $F^{25}G$ mutant likely lost its ability to bind and retain cdc2 in cytoplasm in response to DNA-damaging treatment.

X-ray scattering analysis. The observation that $L^{12}G$ mutant has residual activity in forming homo-dimers and contributing to drug resistance prompted us to further analyze the distribution of monomers vs dimers using small angle x-ray scattering (SAXS) approach, which can be used to quantify the molecular weight for a

single component system and concentration of individual components in a mixture. For a single component system, the forward scattering relates with the molecular weight of a protein by $Io/C_{mass} = k \times Mw$, where C_{mass} is the mass concentration (e.g., in mg/ml) and k is a constant (31). If a system has more than one component, the apparent forward scattering will be the summation of that of individual components, i.e., $Io\_app = \sum_j Io_j$. For a monomer-dimer mixture, the apparent forward scattering relates with the percentage (x) of dimer in mass concentration as a function of $Io_{app} = 0.5k\ Mw_{dimer}(1 + x)$, which is used to estimate the percentage of dimers in solution.

For SAXS determination, we engineered the mutations for production and purification of recombinant proteins (Fig. 8A). Because the $F^{25}G$ mutant does not form any homo-dimers and has no detectable function (see above), we performed SAXS analysis only on purified $L^{25}G$ and $Y^{84}G$ mutants in comparison with the wild type 14-3-3σ protein (Fig. 8B). Assuming that all molecules of the wild type 14-3-3σ protein are dimeric, $L^{12}G$ and $Y^{84}G$ were estimated to have 76% and 58% molecules in dimeric form, respectively, using the above equation. The less dimeric form for $Y^{84}G$ compared with $L^{12}G$ in solution is also supported by its smaller apparent Rg (Fig. 8C) and shorter-distance shifted PDDF than that of $L^{12}G$ (Fig. 8D).

X-ray scattering (small- and wide-angle) measures the protein structural details at various levels (32). The small-angle region, i.e., $q<0.3$ Å^{-1}, delineates the global shape of the protein, while the wide -angle data reflect the tertiary structure (ca. $0.3<q<1.0$ Å^{-1}) and features within secondary structure motifs (ca. $1.0 < q < 2.0$ Å^{-1}). The changes in the small-angle region for the mutants are likely due to existence of monomers of the mutant proteins (Fig. 8B). However, in the wide-angle region, the scattering profiles of mutants are almost identical to that of the wild-type protein, with both resembling the simulated curves for MD structure models, indicating that the mutations do not alter the three-dimensional structures of the protein.

Discussion

In this study, we investigated the role of four interfacial amino acid residues (Leu^{12}, Phe^{25}, Val^{81}, and Tyr^{84}) in 14-3-3σ dimerization and if 14-3-3σ function requires the dimerization status. We found that while the interfacial hydrophobic core residues Leu^{12} and Tyr^{84} played important roles in 14-3-3σ dimerization, the non-core residue Phe^{25} appeared to be more important in controlling 14-3-3σ dimerization activity. Interestingly, a similar non-core residue Val^{81} was less important than Phe^{25} in contribution to 14-3-3σ dimerization. Furthermore, dissociating dimeric 14-3-3σ into monomers by mutating the important dimerization residues Leu^{12}, Phe^{25}, or Tyr^{84} significantly diminished the function of 14-3-3σ in resisting drug-induced apoptosis and in arresting cells at G_2/M phase in response to DNA-damaging treatments and, thus, in drug and radiation resistance.

Although both $L^{12}G$ and $Y^{84}G$ mutants retain some affinity to itself, neither could potentially form detectable dimers with wild type or with the $F^{25}G$ mutant 14-3-3σ. These two mutants could also dimerize between each other and form $L^{12}G/Y^{84}G$ hetero-dimers. It appears that the dimerization affinity of 14-3-3σ molecules occur in the following order: WT/WT > $L^{12}G/L^{12}G$ > $Y^{84}G/Y^{84}G$ ≈ $L^{12}G/Y^{84}G$ > $F^{25}G/F^{25}G$ ≈ $L^{12}G/F^{25}G$ ≈ $Y^{84}G/F^{25}G$ ≈ WT/mutants. This order of observation is interesting and may be due to the fact that wild type has a much higher dimerization activity than any mutants and, thus, kinetically more favorable to form dimers with wild type than to mutant molecules when both wild type and mutant molecules are present. Mutant molecules, on the other

hand, have low dimerization activity and, thus, form less dimers between themselves than wild type to wild type. Consistent with this observation, the calculated binding energies from MD simulation for wild type/wild type and mutant/mutant dimers are also in the same order (19). The $F^{25}G$ mutant appears to have lost all of its ability to dimerize with itself or with wild type and other mutant 14-3-3σ molecules. Thus, the Phe^{25} residue is very critical to 14-3-3σ dimerization. These findings also suggest that disrupting the function of Phe^{25} by small molecules may be able to completely dissociate 14-3-3σ dimerization and that it may be targeted for drug discovery.

It is noteworthy that the $V^{81}G$ mutant behaves very differently from the $F^{25}G$ mutant although both have similar buried surface areas upon dimerization and not localized in the interfacial core (Table 2). While the $F^{25}G$ mutant completely lost its dimerization activity with itself, other mutants, or the wild type protein, the $V^{81}G$ mutant retains activity to hetero-dimerize with the wild type 14-3-3σ. Previously, we found that mutation of Phe^{25} caused disruption of the dimeric interface and shifting of side chains of Lys^{9}. However, mutation of Val^{81} does not appear to affect hydrophobic core residues in the dimeric interface as revealed by structural analysis using MD simulation. It is also noteworthy that the two subareas of the dimeric interface are both important and one intact subarea does not appear to be sufficient to maintain the full dimerization activity. In fact, the mutant proteins carrying mutations in the same subarea (e.g., $L^{12}G/Y^{84}G$ heterodimer) did not form more dimers than the ones with mutations in both subareas (e.g., $L^{12}G/L^{12}G$) (see Fig. 4A). Thus, we conclude that both subareas of the dimeric interface are required to maintain a full dimerization activity of 14-3-3σ and maintaining one intact subarea has no advantage over mutations in both subareas.

In functional studies, we found that the $L^{12}G$ mutant has detectable activity in causing resistance, change in apoptosis and G_2/M arrest. This finding is interesting in that the $L^{12}G$ mutant has the highest activity in formation of $L^{12}G/L^{12}G$ homo-dimers among the three mutants tested, confirming that dimerization status is required for the function of 14-3-3σ. It is noteworthy that the drug resistance activity of $L^{12}G$ mutant is much less than the wild type protein although 76% of purified $L^{12}G$ is estimated to exist as homo-dimers. This discrepancy may be due to over-estimation of homo-dimers for the mutant molecule because it was calculated with an assumption that 100% of wild type 14-3-3σ exists as homo-dimers, which is unlikely the case (see Fig. 2). Potential non-specific interactions at high concentrations of purified proteins for SAXS determination may also contribute to the higher estimation of homo-dimeric mutant molecules. Nevertheless, lower level (58%) of homo-dimers for the $Y^{84}G$ mutant was detected, consistent with the observation using co-IP and its lack of drug resistance activity. Alternatively, the above discrepancy may also be due to the possibility that the mutations directly affect the functionality of the protein in addition to its effect on dimerization. However, because 14-3-3σ exerts its activity by functioning as a chaperone to bind to its ligand proteins and these mutations are far away from the ligand-binding site, it is unlikely that these mutations have any direct effect on ligand-binding activity of 14-3-3σ. Indeed, MD simulation analysis showed that these mutations do not affect the conformation of the ligand-binding domain of 14-3-3σ (19) although these observations of computational analyses have not yet been validated experimentally. However, the data from wide-angle x-ray scaterring analyses of the purified recombinant proteins suggest that

these mutations do not cause major conformational change to 14-3-3σ.

Previously, it was found that the monomeric mutant of drosophila 14-3-3ζ appears to be functional and may still bind to its drosophila ligand Slob (33). However, in another study of mammalian 14-3-3ζ, it was found that dimerization of 14-3-3ζ is dependent on the phosphorylation of the Ser^{58} (34), which is absent in 14-3-3σ, and the dimerization is required for its activity in binding phosphorylated peptides and protein ligands (35). Interestingly, the dimerization deficient 14-3-3ζ is able to bind to unphosphorylated proteins. In our study, we also observed that the $F^{25}G$ mutant 14-3-3σ can still bind to a group of proteins (unpublished observations) despite the fact that it cannot form homo-dimers. It is, thus, possible that the dimerization deficient mutant 14-3-3σ is unable to bind to its natural phosphorylated protein ligands to exert its normal functions in contributing drug and radiation resistance due to binding to other proteins. This is supported by the observation that the $F^{25}G$ mutant lost its ability to bind and arrest cdc2 in cytoplasm in response to DNA damage. Clearly, further work is needed to test this possibility.

In summary, both intact subareas of the dimeric interface appear to be required to maintain the full dimerization activity of 14-3-3σ and mutation of hydrophobic core residues in any one of these subareas diminishes the dimerization activity. In addition to the core residues, the non-core residue Phe^{25} also plays an important role in driving 14-3-3σ dimerization by organizing other hydrophobic core residues. However, another similar non-core residue Val^{81} is much less important and its mutation does not affect the dimerization activity of 14-3-3σ. The dimerization deficient 14-3-3σ also lost their function in causing drug and radiation resistance. Based on these findings, it is tempting to speculate that targeting any one of these important residues may help identify inhibitors that can disrupt 14-3-3σ dimerization for drug discovery to sensitize 14-3-3σ-mediated resistance in cancer treatments. The outcome of this study may help drug the "undruggable" oncogenic protein dimers in general.

Acknowledgement

The authors wish to thank for the use of the Advanced Photon Source, an Office of Science User Facility operated for the U.S. Department of Energy (DOE) Office of Science by Argonne National Laboratory, which was supported by the U.S. DOE under Contract No. DE-AC02-06CH11357.

REFERENCES

1. Li, Z., Liu, J.-Y., and Zhang, J.-T. (2009) *American Journal of Translational Research* **1**, 326-340
2. Morrison, D. K. (2009) *Trends Cell Biol* **19**, 16-23
3. Fu, H., Subramanian, R. R., and Masters, S. C. (2000) *Annu Rev Pharmacol Toxicol* **40**, 617-647
4. Benzinger, A., Muster, N., Koch, H. B., Yates, J. R., 3rd, and Hermeking, H. (2005) *Mol Cell Proteomics* **4**, 785-795
5. Wilker, E. W., van Vugt, M. A., Artim, S. A., Huang, P. H., Petersen, C. P., Reinhardt, H. C., Feng, Y., Sharp, P. A., Sonenberg, N., White, F. M., and Yaffe, M. B. (2007) *Nature* **446**, 329-332
6. Chan, T. A., Hermeking, H., Lengauer, C., Kinzler, K. W., and Vogelstein, B. (1999) *Nature* **401**, 616-620

7. Laronga, C., Yang, H. Y., Neal, C., and Lee, M. H. (2000) *J Biol Chem* **275**, 23106-23112
8. Han, B., Xie, H., Chen, Q., and Zhang, J. T. (2006) *Mol Cancer Ther* **5**, 903-912
9. Hermeking, H., and Benzinger, A. (2006) *Seminars in cancer biology* **16**, 183-192
10. Samuel, T., Weber, H. O., Rauch, P., Verdoodt, B., Eppel, J. T., McShea, A., Hermeking, H., and Funk, J. O. (2001) *J Biol Chem* **276**, 45201-45206
11. Chu, K., Teele, N., Dewey, M. W., Albright, N., and Dewey, W. C. (2004) *Radiat Res* **162**, 270-286
12. Neupane, D., and Korc, M. (2008) *Clin Cancer Res* **14**, 7614-7623
13. Ferguson, A. T., Evron, E., Umbricht, C. B., Pandita, T. K., Chan, T. A., Hermeking, H., Marks, J. R., Lambers, A. R., Futreal, P. A., Stampfer, M. R., and Sukumar, S. (2000) *PNAS* **97**, 6049-6054
14. Vercoutter-Edouart, A.-S., Lemoine, J., Le Bourhis, X., Louis, H., Boilly, B., Nurcombe, V., Revillion, F., Peyrat, J.-P., and Hondermarck, H. (2001) *Cancer Res* **61**, 76-80
15. Liu, Y., Liu, H., Han, B., and Zhang, J. T. (2006) *Cancer Res* **66**, 3248-3255
16. Zhang, J. T., and Liu, Y. (2007) *Cancer Treat Rev* **33**, 741-756
17. Wilker, E. W., Grant, R. A., Artim, S. C., and Yaffe, M. B. (2005) *J Biol Chem* **280**, 18891-18898
18. Verdoodt, B., Benzinger, A., Popowicz, G. M., Holak, T. A., and Hermeking, H. (2006) *Cell Cycle* **5**, 2920-2926
19. Liu, J. Y., Li, Z., Li, H., and Zhang, J. T. (2011) *J Chem Inf Model* **51**, 2612-2625
20. Li, Z., Dong, Z., Myer, D., Yip-Schneider, M., Liu, J., Cui, P., Schmidt, C. M., and Zhang, J. T. (2010) *BMC Cancer* **10**, 598
21. Yang, Y., Chen, Q., and Zhang, J. T. (2002) *J Biol Chem* **277**, 44268-44277
22. Zhang, J. T., Han, E., and Liu, Y. (2000) *Journal of Cell Science* **113**, 2545-2555
23. Dong, Z., Liu, Y., and Zhang, J. T. (2005) *Nucleic Acids Res* **33**, 2715-2725
24. Yang, Y., Mo, W., and Zhang, J. T. (2010) *Biochemistry* **49**, 10854-10861
25. Mo, W., Qi, J., and Zhang, J. T. (2012) *Biochemistry* **51**, 3634-3641
26. Xu, J., Peng, H., Chen, Q., Liu, Y., Dong, Z., and Zhang, J. T. (2007) *Cancer Res* **67**, 4373-4381
27. Dong, Z., Liu, Z., Cui, P., Pincheira, R., Yang, Y., Liu, J., and Zhang, J. T. (2009) *Exp Cell Res* **315**, 1889-1894
28. Onufriev, A., Bashford, D., and Case, D. A. (2000) *J Phys Chem B* **104**, 3712-3720
29. Glatter, O., and Kratky, O. (1982) *Small Angle X-ray Scattering*, Academic Press Inc., New York
30. Svergun, D. I. (1992) *J. Appl. Cryst.* **25**, 495-503
31. Mylonas, E., and Svergun, D. I. (2007) *Journal of Applied Crystallography* **40**, S245-S249
32. Hirai, M., Koizumi, M., Hayakawa, T., Takahashi, H., Abe, S., Hirai, H., Miura, K., and Inoue, K. (2004) *Biochemistry* **43**, 9036-9049
33. Zhou, Y., Reddy, S., Murrey, H., Fei, H., and Levitan, I. B. (2003) *J Biol Chem* **278**, 10073-10080
34. Woodcock, J. M., Murphy, J., Stomski, F. C., Berndt, M. C., and Lopez, A. F. (2003) *J Biol Chem* **278**, 36323-36327
35. Shen, Y. H., Godlewski, J., Bronisz, A., Zhu, J., Comb, M. J., Avruch, J., and Tzivion, G. (2003) *Mol Biol Cell* **14**, 4721-4733

FOOTNOTES

*This work was supported in part by the National Institutes of Heath grant R01 CA140582 (JTZ) and by an IUPUI iM^{2}CS grant (JYL).

‡Current address: Department of Molecular Immunology, Institute of Basic Medical Sciences, 27 Taiping Road, Beijing 100850, P. R. China

FIGURE LEGENDS

Figure 1. **Interaction between mutant and wild type 14-3-3σ.** A. Schematic diagram of tagged 14-3-3σ constructs and dimeric 14-3-3σ molecules with mutated residues indicated. A 14-3-3σ dimer has two equivalent subareas in the interface with 180^{o} symmetry. B and C. Interaction between HA-tagged wild type and HAM_2-tagged mutant 14-3-3σ molecules in whole cell (B) and cell-free (C) systems. HEK293 cells with stable expression of HA-tagged wild type 14-3-3σ were transiently transfected with HAM_2-tagged wild type or mutant 14-3-3σ (B) or both HA- and HAM_2-tagged wild type and mutant 14-3-3σ transcripts were co-translated in rabbit reticulocyte lysates (C) as indicated followed by co-immunoprecipitation with Myc antibody. The precipitates were then subjected to Western blot analysis probed with HA antibodies to detect both HAM_2- and HA-tagged proteins. The asterisks indicate the co-precipitated HA-tagged wild type 14-3-3σ proteins. The broad bands for $L^{12}G$, $F^{25}G$, $V^{81}G$, and $Y^{84}G$ mutant proteins shown in panel B are likely due to degradation.

Figure 2. **Non-denaturing PAGE analysis of dimerization activity of wild type and Phe^{25} mutant 14-3-3σ**. HAM_2- and HA-tagged wild type and mutant 14-3-3σ transcripts were co-translated in rabbit reticulocyte lysate followed by separation of the products using non-denaturing PAGE and Western blot analysis of dimeric and monomeric 14-3-3σ proteins probed with HA (upper panel) or Myc (lower panel) antibodies for HA- and HAM_2-tagged molecules. The asterisks indicate wild type HAM_2/HAM_2 (upper band) HAM_2/HA (middle band), and HA/HA (lower band) 14-3-3σ dimers with different mobility due to different sizes of the tags used.

Figure 3. RMSF of core residues in both subunits. Amino acid residues that constitute hydrophobic cores are indicated at the top. Single underlined residues are for core I and double underlined ones are for core II.

Figure 4. Homo- and hetero-dimerization between the mutant 14-3-3σ proteins. A. Schematic diagram of the relative position of mutations in the two subareas of the interface between homo- and hetero-mutant 14-3-3σ dimers. B and C. Homo- (B) and hetero- (C) dimerization of mutant 14-3-3σ. Mia PaCa-2 cells with sable expression of Flag-tagged wild type or mutant 14-3-3σ were transiently transfected with or without Myc-tagged wild type or mutant 14-3-3σ as indicated followed by immunoprecipitation with Flag antibody. The precipitates were then subjected to Western blot analysis probed with Flag or Myc antibody.

Figure 5. Dimerization is required for 14-3-3σ-mediated drug resistance. A. Western blot analysis of stable PaCa-2 cell lines transfected with vector (Vec) control, wild type and mutant 14-3-3σ. Actin was used as a loading control. B, C, and D. Survival analysis. Stable cell lines as shown in panel A were treated with different concentrations of mitoxantrone (MXT, B and C) or with or without 2 Gy γ-irradiation (D) followed by SRB assay (B and C) or colony formation assay (D). Panel B represents a typical experiment of survival assay. Panels C and D are summary of 3-4 experiments. RRF=relative resistance factor=$IC_{50(MXT)}/IC_{50(Vec)}$. *$p<0.05$, **$p<0.01$.

Figure 6. Effect of dimerization deficiency on drug-induced apoptosis. A. Western blot analysis of PARP cleavage in stable PaCa-2 cell lines transfected with vector (Vec) control, wild type and mutant 14-3-3σ following mitoxantrone treatment at different times. B. Quantitative analysis of cleaved PARP. The intact (115 kDa) and cleaved (85 kDa) PARP shown in panel A was quantified using a gel densitometer and the ratio of 85 kDa/Total (85 kDa+115 kDa) was calculated to serve as an indicator of apoptosis.

Figure 7. Effect of dimerization deficiency on drug-induced G2/M arrest. A. FACS analysis of cell cycle distribution of stable PaCa-2 cell lines transfected with vector (Vec) control, wild type and mutant 14-3-3σ following treatment with 10 nM mitoxantrone (MXT) or DMSO control for 3 days. B. Quantitative analysis of cell cycle distribution as shown in panel A. C. Immunoflurescence staining of cdc2. PaCa-2 cells with stable expression of wild type (WT) and mutant ($F^{25}G$) 14-3-3σ were treated with DMSO control or 10 nM mitoxantrone (MXT) for 3 days followed by immunofluorescence staining of cdc2.

Figure 8. Purification and x-ray scattering analyses of wild type and mutant 14-3-3σ proteins. A. SDS-PAGE profiles of purified wild type, $L^{12}G$, and $Y^{84}G$ mutant 14-3-3σ stained with commassie blue. B. Small- and wide-angle x-ray scattering profiles for wide-type and mutant 14-3-3σ proteins. The black and cyan lines represent simulated profiles of dimeric and monomeric molecules, respectively, generated using MD simulation. The red, blue, and green lines represent profiles of wild-type, $L^{12}G$ and Y84G mutant molecules, respectively, determined using x-ray scattering. The profiles were vertically offset for clarity. C. Guinier plots of wild-type (red), $L^{12}G$ (blue) and $Y^{84}G$ (green) mutants using scattering data from panel B normalized by mass concentration. D. Normalized pair distance distribution functions (PDDF) of wild-type (red), $L^{12}G$ (blue) and $Y^{84}G$ (green) mutant 14-3-3σ. The PDDFs were calculated with program GNOM using scattering data (q range up to $0.3Å^{-1}$ from panel B.

Table 1. Primers used for engineering 14-3-3σ constructs

Tags/Mutations	Primers
Flag	5'-GGAATTCATGGAGAGAGCCAGTCTG-3'
	5'-GCTCGAGTCACTTGTCATCGTCGTCCTTGTAGTCGCTCTGGGGCTCCTGGGGAGC-3'
HA	5'-GGAATTCATGGAGAGAGCCAGTCTG-3'
	5'-GCTCGAGTCAGAGGCTAGCATAATCAGGAACATCATACGGATAGCTCTGGGGCTCCTGGGGAGC-3'
Myc	5'-GGAATTCATGGAGAGAGCCAGTCTG-3'
	5'-GCTCGAGTCACAGATCTTCTTCAGAAATAAGTTTTTGTTCGCTCTGGGGCTCCTGGGGAGC-3'
HAM_2	5'-GGAATTCATGGAGAGAGCCAGTCTG-3'
	5'-GCTCGAGTCACAGATCTTCTTCAGAAATAAGTTTTTGTTCCAGATCTTCTTCAGAAATAAGTTTTTGT
	TCGAGGCTAGCATAATCAGG-3'
Q^8G	5'-GGAATTCATGGAGAGAGCCAGTCTG-3'
	5'-ATGGAGAGAGCCAGTCTGATCGGGAAGGCCAAGCTGGCAGAGC-3'
$L^{12}G$	5'-ATGGAGAGAGCCAGTCTGATCCAGAAGGCCAAGGGGGCAGAGCAGGCCGAACG-3'
	5'-CGTTCGGCCTGCTCTGCCCCCTTGGCCTTCTGGATCAGACTGGCTCTCTCC-3'
$F^{25}G$	5'-ATGAGGACATGGCAGCCGGCATGAAAGGCGCCGTGGA-3'
	5'-CCACGGCGCCTTTCATGCCGGCTGCCATGTCCTC-3'
$F^{25}E$	5'-ATGAGGACATGGCAGCCGAGATGAAAGGCGCCGTGGA-3'
	5'-CCACGGCGCCTTTCATCTCGGCTGCCATGTCCTC-3'
$V^{81}G$	5'-CGGAGGAGAAGGGGCCCGAGGGGCGTGAGTACCGGGAGAAGG-3'
	5'-CCTTCTCCCGGTACTCACGCCCCTCGGGCCCCTTCTCCTCCG-3'
$Y^{84}G$	5'-GGGCCCGAGGTGCGTGAGGGCCGGGAGAAGGTGGAGAC-3'
	5'-GTCTCCACCTTCTCCCGGCCCTCACGCACCTCGGGCCC-3'

Table 2. Residues important for dimer formation

Rankings[a]	Residues	Buried Surface Area[b]	Core vs non-Core
1	TYR^{84}	120 (99%)	Core
2	LEU^{12}	88 (96%)	Core
3	ALA^{16}	58 (91%)	Core
4	LYS^{9}	70 (83%)	Core
5	ALA^{58}	36 (100%)	Core
6	LEU^{62}	25 (100%)	Core
7	PHE^{25}	25 (53%)	non-Core
8	VAL^{81}	24 (42%)	non-Core
9	GLN^{8}	23 (25%)	non-Core
10	VAL^{88}	14 (100%)	Core
11	ALA^{13}	9 (100%)	Core

[a]The rankings are based on buried surface areas at the dimeric interface each residue provides.
[b]Buried surface areas, in A^2, represents the surface area that becomes buried upon dimerization. The percentage of buried surface area=Surface area that becomes buried upon dimerization/Total solvent accessible area in monomer*100. .

Figure 1.

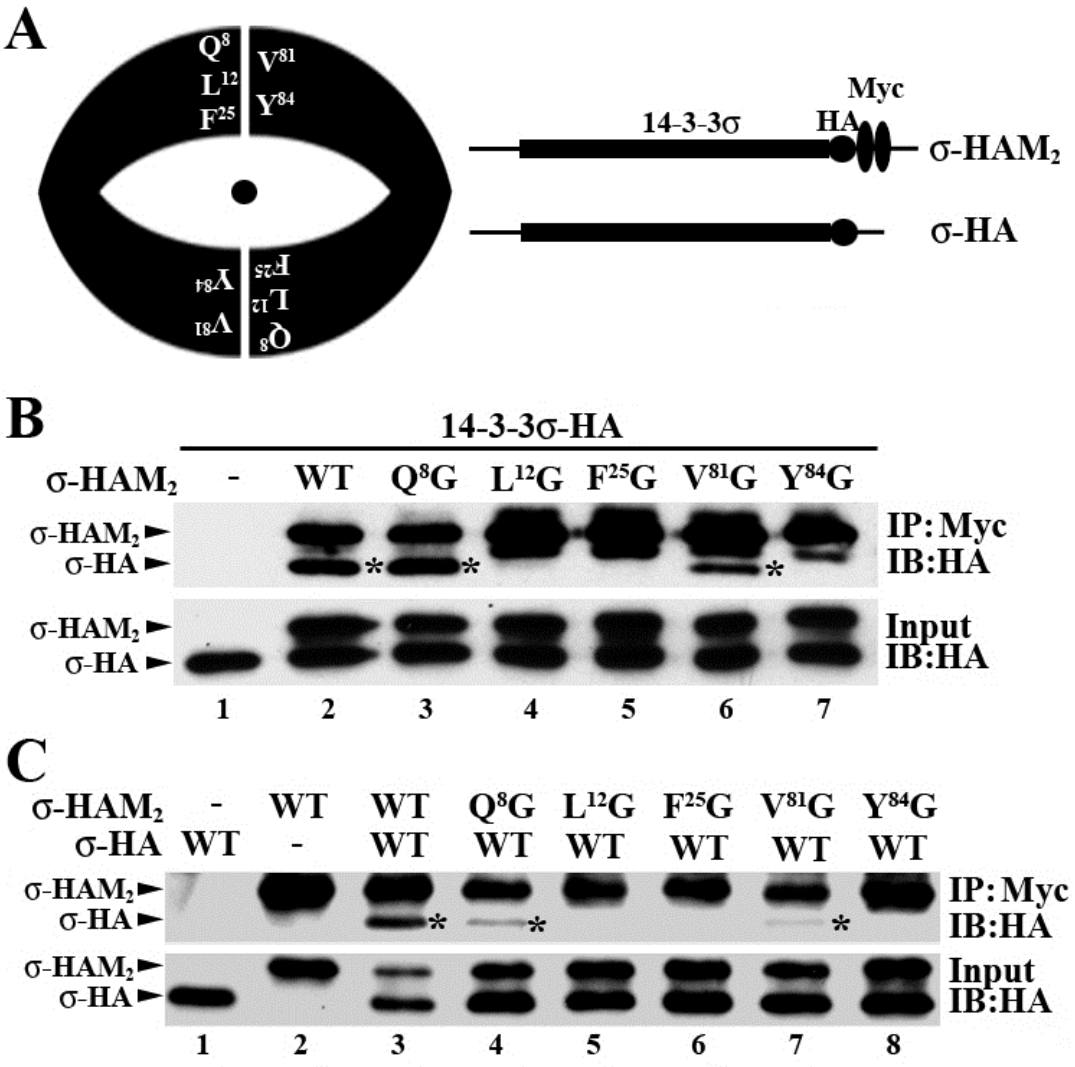
A
Q8
L12
F25
V81
Y84
14-3-3σ
Myc
HA
σ-HAM2
σ-HA
B
14-3-3σ-HA
σ-HAM2 - WT Q8G L12G F25G V81G Y84G
σ-HAM2
σ-HA
IP: Myc
IB:HA
Input
IB:HA
1 2 3 4 5 6 7
C
σ-HAM2 - WT WT Q8G L12G F25G V81G Y84G
σ-HA WT - WT WT WT WT WT WT
IP: Myc
IB:HA
Input
IB:HA
1 2 3 4 5 6 7 8

Figure 2.

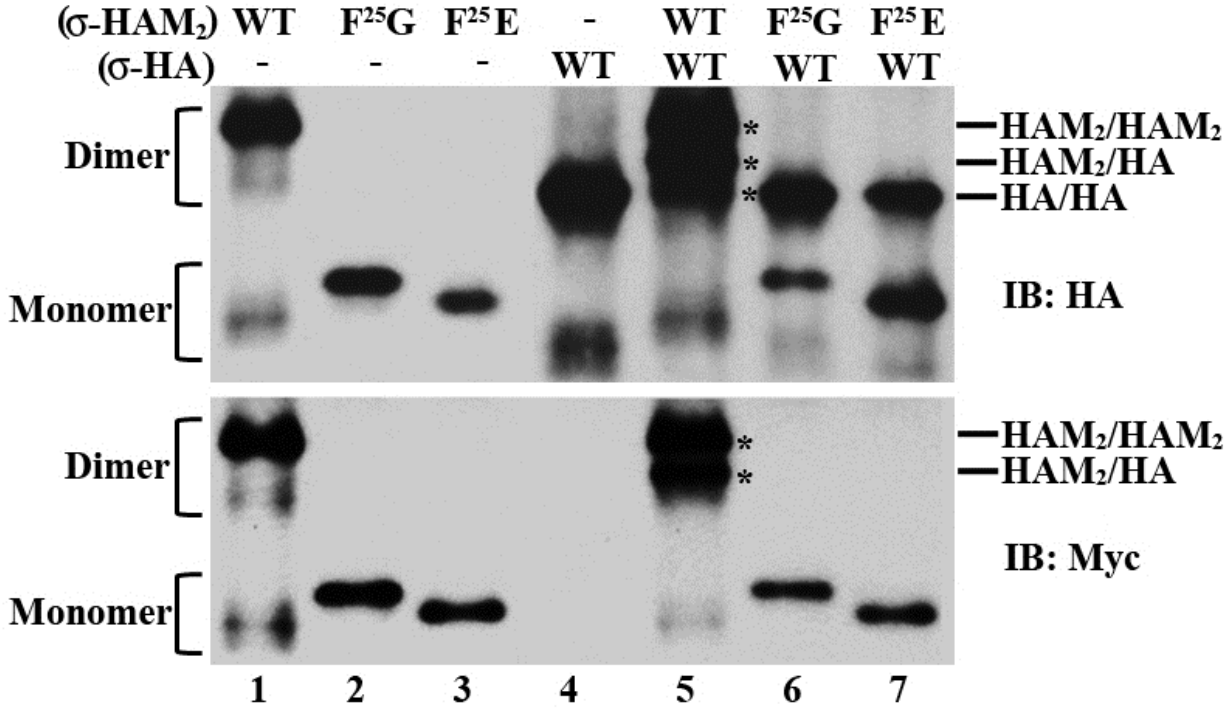
(σ-HAM2) WT F25G F25E - WT F25G F25E
(σ-HA) - - - WT WT WT WT
Dimer
Monomer
HAM2/HAM2
HAM2/HA
HA/HA
IB: HA
Dimer
Monomer
HAM2/HAM2
HAM2/HA
IB: Myc
1 2 3 4 5 6 7

Figure 3.

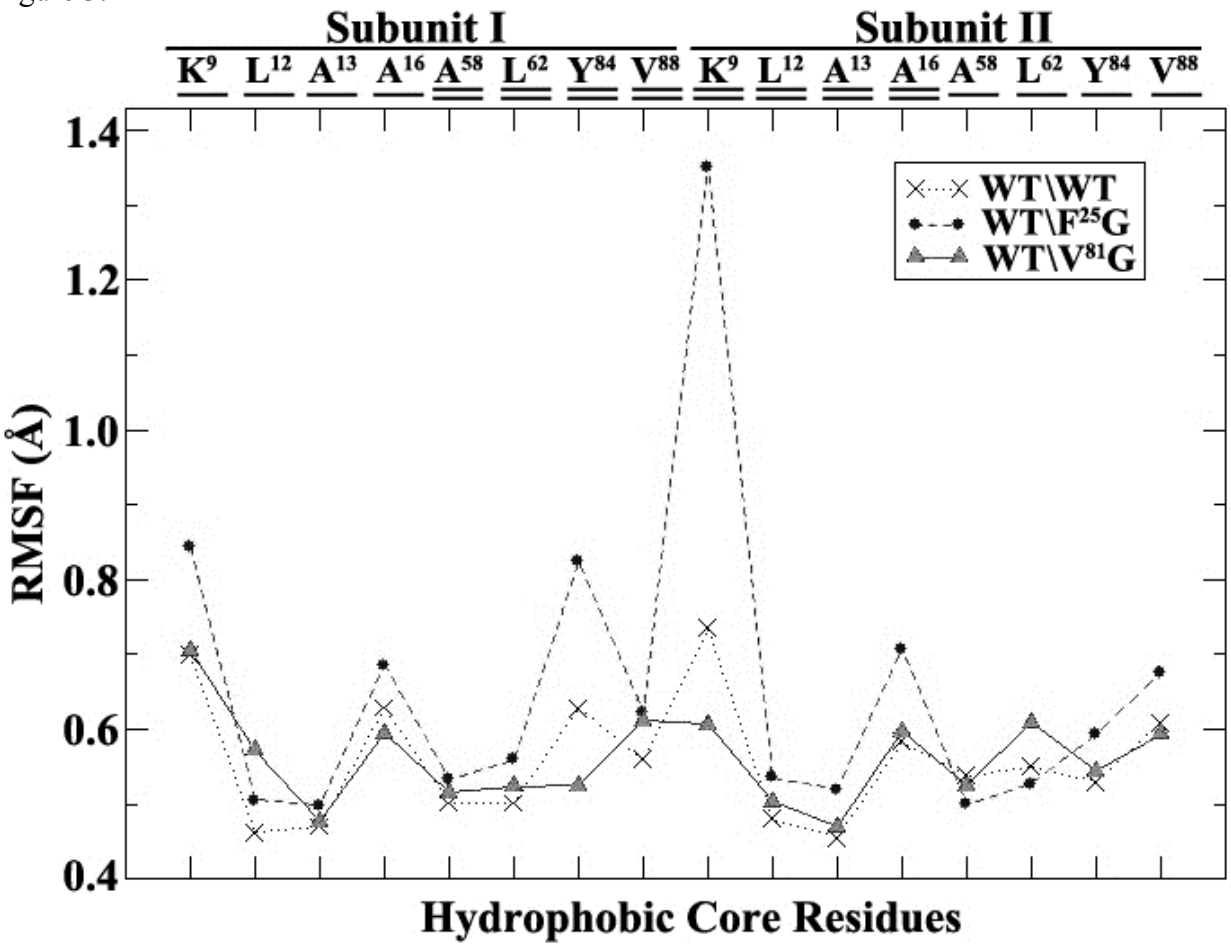
Subunit I
Subunit II
K9 L12 A13 A16 A58 L62 Y84 V88
K9 L12 A13 A16 A58 L62 Y84 V88
WT\WT
WT\F25G
WT\V81G
RMSF (Å)
1.4
1.2
1.0
0.8
0.6
0.4
Hydrophobic Core Residues

Figure 4.

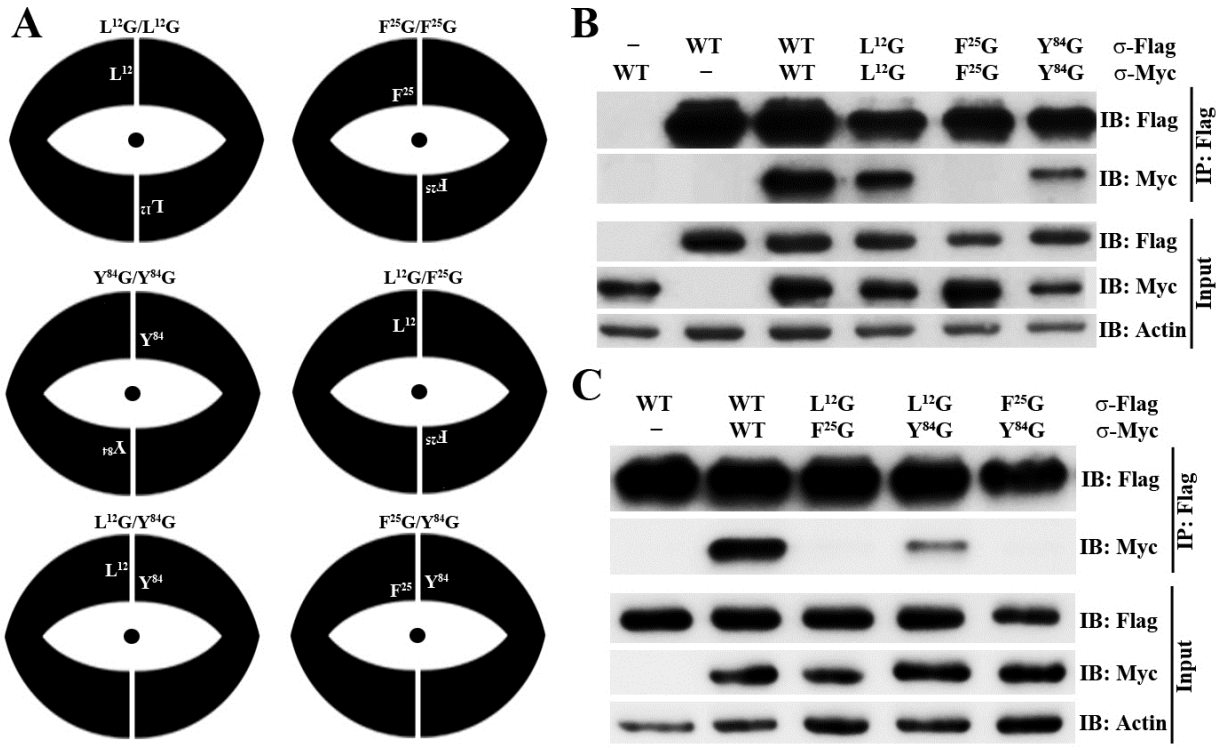
A
L12G/L12G
F25G/F25G
Y84G/Y84G
L12G/F25G
L12G/Y84G
F25G/Y84G
B
WT
WT
WT
L12G
F25G
Y84G
σ-Flag
σ-Myc
IB: Flag
IB: Myc
IP: Flag
IB: Flag
IB: Myc
IB: Actin
Input
C
WT
WT
L12G
L12G
F25G
σ-Flag
WT
F25G
Y84G
Y84G
σ-Myc
IB: Flag
IB: Myc
IP: Flag
IB: Flag
IB: Myc
IB: Actin
Input

Figure 5.

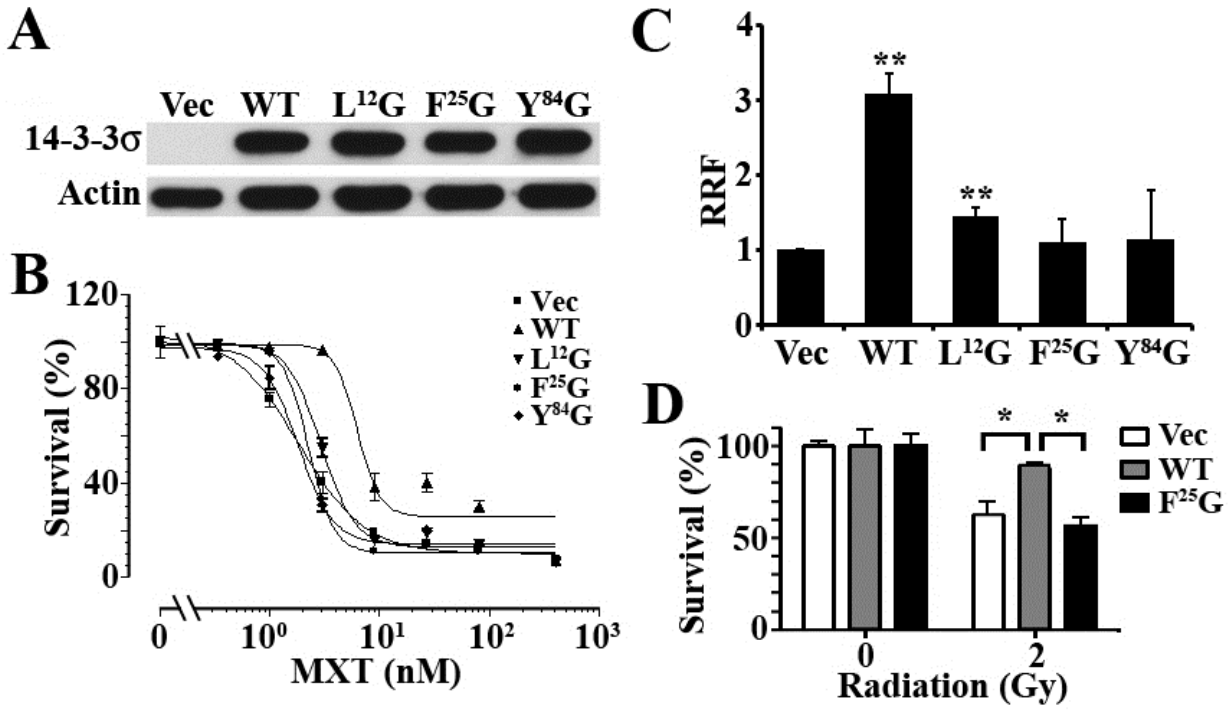
A
Vec
WT
L12G
F25G
Y84G
14-3-3σ
Actin
B
120
80
40
0
Survival (%)
Vec
WT
L12G
F25G
Y84G
0
10^0
10^1
10^2
10^3
MXT (nM)
C
4
3
2
1
0
RRF
**
**
Vec
WT
L12G
F25G
Y84G
D
100
50
0
Survival (%)
*
*
Vec
WT
F25G
0
2
Radiation (Gy)

Figure 6.

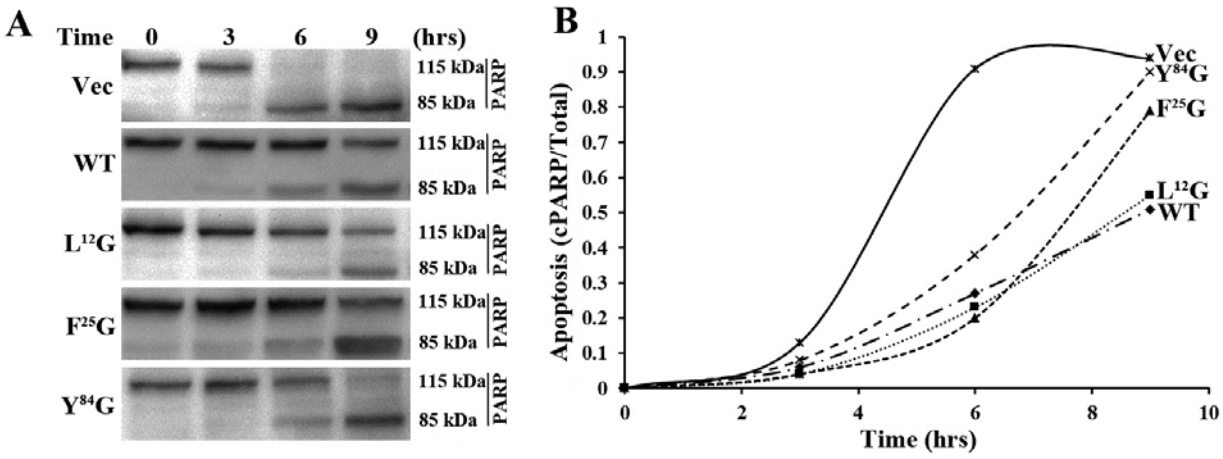
A
Time 0 3 6 9 (hrs)
Vec
WT
L12G
F25G
Y84G
115 kDa
85 kDa
PARP
B
Apoptosis (cPARP/Total)
Time (hrs)
Vec
Y84G
F25G
L12G
WT

Figure 7.

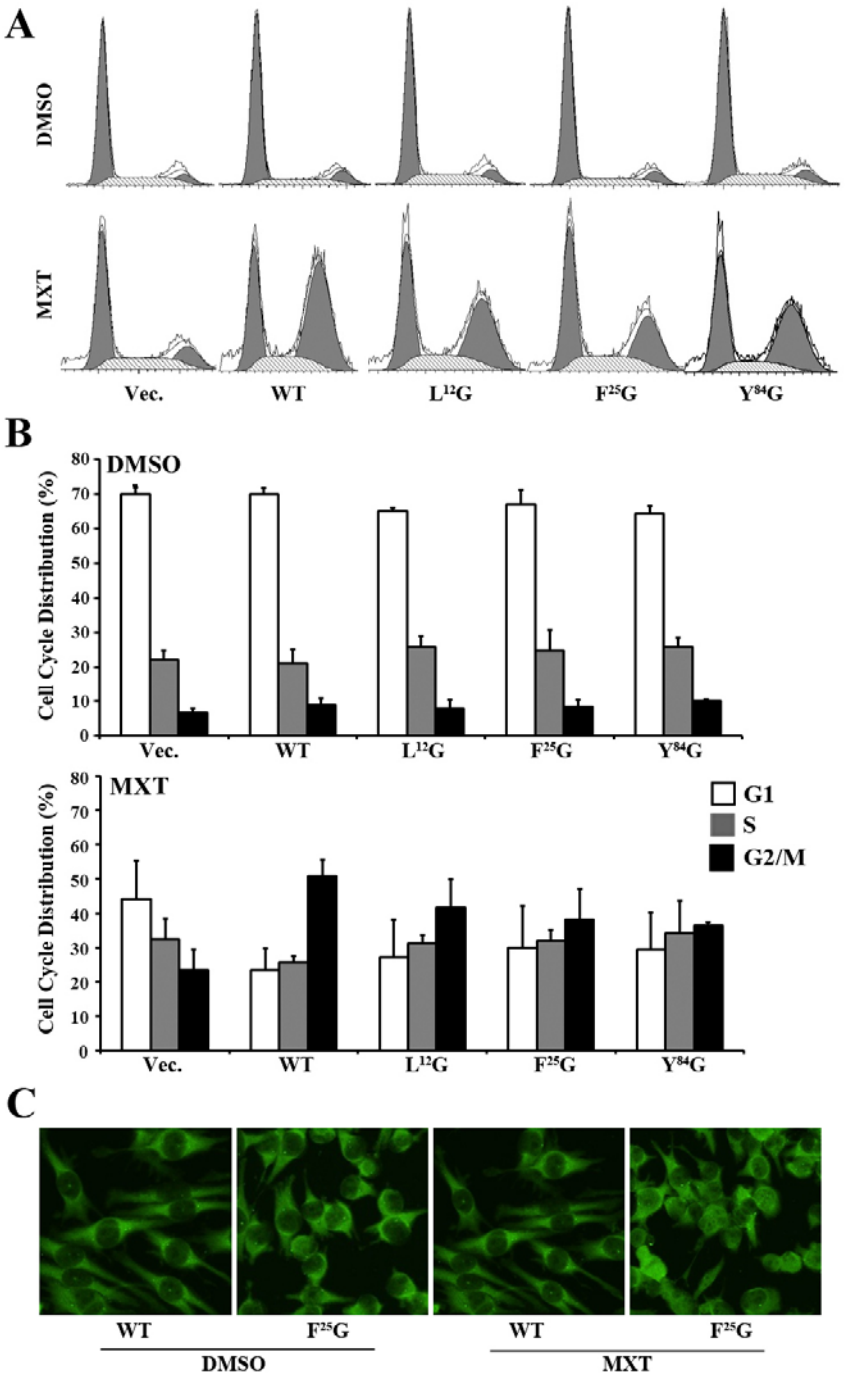
A
DMSO
MXT
Vec.
WT
L12G
F25G
Y84G
B
DMSO
Cell Cycle Distribution (%)
MXT
G1
S
G2/M
C
WT
F25G
DMSO
MXT

Figure 8.

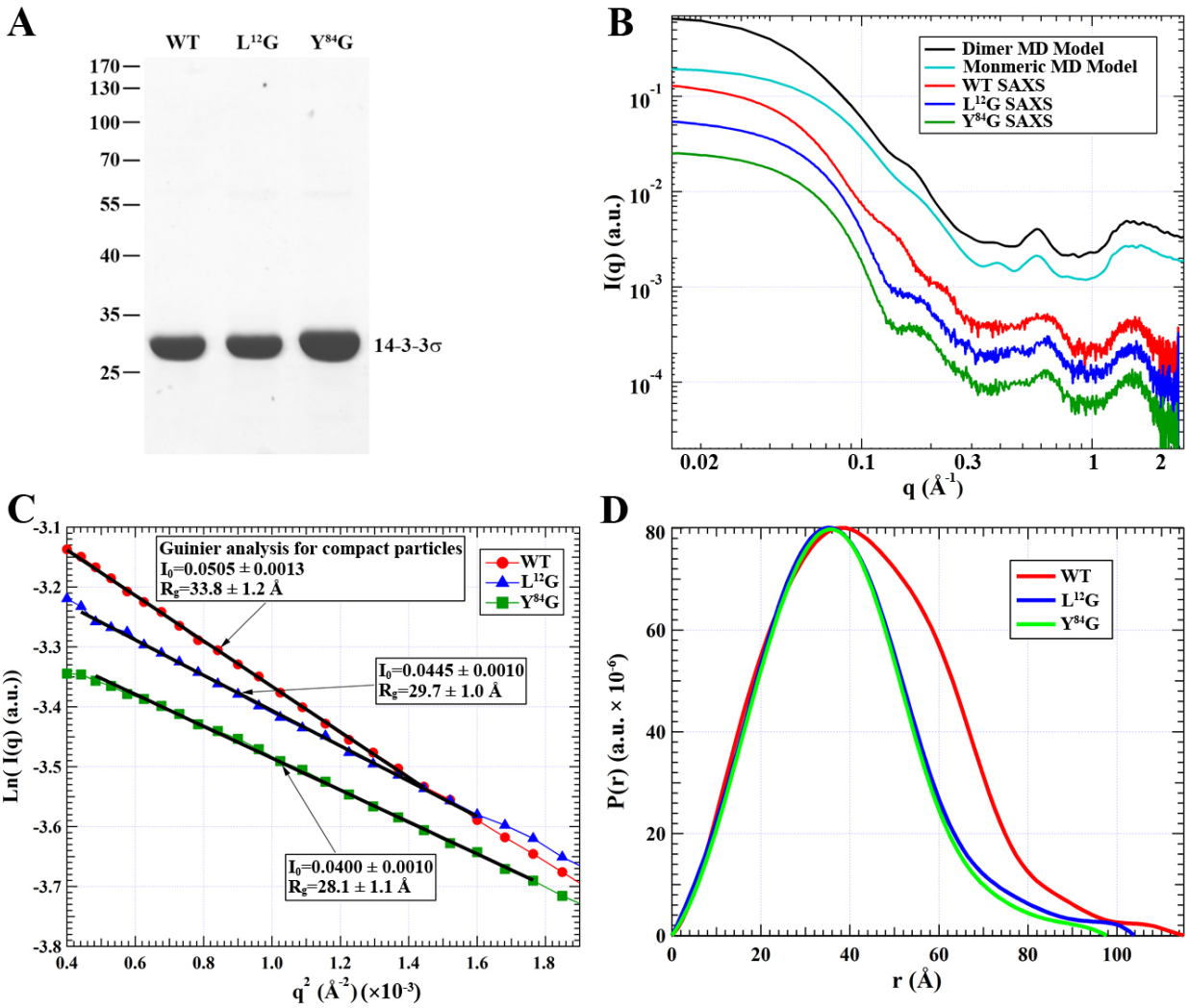
A
WT
L12G
Y84G
170
130
100
70
55
40
35
25
14-3-3σ
B
Dimer MD Model
Monmeric MD Model
WT SAXS
L12G SAXS
Y84G SAXS
I(q) (a.u.)
q (Å-1)
C
Guinier analysis for compact particles
I0=0.0505 ± 0.0013
Rg=33.8 ± 1.2 Å
I0=0.0445 ± 0.0010
Rg=29.7 ± 1.0 Å
I0=0.0400 ± 0.0010
Rg=28.1 ± 1.1 Å
WT
L12G
Y84G
Ln(I(q) (a.u.))
q2 (Å-2) (×10-3)
D
WT
L12G
Y84G
P(r) (a.u. × 10-6)
r (Å)

Protein Structure and Folding:

Determinants of 14-3-3σ dimerization and function in drug and radiation resistance

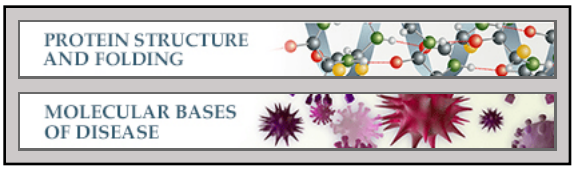

Zhaomin Li, Hui Peng, Li Qin, Jing Qi, Xiaobing Zuo, Jing-Yuan Liu and Jian-Ting Zhang

J. Biol. Chem. *published online September 16, 2013*

Access the most updated version of this article at doi: 10.1074/jbc.M113.467753